Biomedicine & Pharmacotherapy 144 (2021) 112373

Contents lists available at ScienceDirect

Biomedicine & Pharmacotherapy

journal homepage: www.elsevier.com/locate/biopha

pH-sensitive doxorubicin-tocopherol succinate prodrug encapsulated in docosahexaenoic acid-based nanostructured lipid carriers: An effective strategy to improve pharmacokinetics and reduce toxic effects

Eduardo Burgarelli Lages [a,b], Renata Salgado Fernandes [a], Marina Mol Sena Andrade [a], Nitchawat Paiyabhroma [b], Renata Barbosa de Oliveira [a], Christian Fernandes [a], Geovanni Dantas Cassali [c], Pierre Sicard [b,d], Sylvain Richard [b,d], André Luís Branco de Barros [e], Lucas Antônio Miranda Ferreira [a,*]

[a] Departamento de Produtos Farmacêuticos, Faculdade de Farmácia, Universidade Federal de Minas Gerais, Belo Horizonte, MG, Brazil
[b] PhyMedExp, Université de Montpellier, INSERM, CNRS, Montpellier, France
[c] Departamento de Patologia Geral, Instituto de Ciências Biológicas, Universidade Federal de Minas Gerais, Belo Horizonte, MG, Brazil
[d] IPAM, BioCampus Montpellier, INSERM, CNRS, Université de Montpellier, Montpellier, France
[e] Departamento de Análises Clínicas e Toxicológicas, Faculdade de Farmácia, Universidade Federal de Minas Gerais, Belo Horizonte, MG, Brazil

ARTICLE INFO

Keywords:
Doxorubicin
Nanomedicine
Ion-pairing
Amide
Hydrazone
Antitumor activity
Cardiotoxicity

ABSTRACT

Side effects often limit the use of doxorubicin (DOX) in cancer treatment. We have recently developed a nanostructured lipid carrier (NLC) formulation for synergistic chemotherapy, encapsulating DOX and the anti-cancer adjuvants docosahexaenoic acid (DHA) and α-tocopherol succinate (TS). Hydrophobic ion-pairing with TS allowed a high DOX entrapment in the nanocarrier. In this work, we investigated the pharmacokinetics of this formulation after intravenous administration in mice. The first data obtained led us to propose synthesizing covalent DOX-TS conjugates to increase DOX retention in the NLC. We successfully conjugated DOX to TS via an amide or hydrazone bond. *In vitro* studies in 4T1 tumor cells indicated low cytotoxicity of the amide derivative, while the hydrazone conjugate was effective in killing cancer cells. We encapsulated the hydrazone derivative in a DHA-based nanocarrier (DOX-hyd-TS/NLC), which had reduced particle size and high drug encapsulation efficiency. The pH-sensitive hydrazone bond allowed controlled DOX release from the NLC, with increased drug release at acidic conditions. *In vivo* studies revealed that DOX-hyd-TS/NLC had a better pharmacokinetic profile than free DOX and attenuated the short-term cardiotoxic effects caused by DOX, such as QT prolongation and impaired left ventricular systolic function. Moreover, this formulation showed excellent therapeutic performance by reducing tumor growth in 4T1 tumor-bearing mice and decreasing DOX-induced toxicity to the heart and liver, demonstrated by hematologic, biochemical, and histologic analyses. These results indicate that DOX-hyd-TS/NLC may be a promising nanocarrier for breast cancer treatment.

1. Introduction

Doxorubicin (DOX) is a cytotoxic anthracycline widely used in chemotherapy due to its efficacy in fighting many cancers, such as carcinomas, sarcomas, and hematologic malignancies. However, its use can result in cumulative and dose-dependent cardiotoxicity as one of the most serious adverse effects, ranging from structural and functional changes in cardiomyocytes to severe cardiomyopathy and congestive heart failure [1,2]. DOX-loaded nanocarriers aim to overcome the challenges associated with cancer therapy, providing a reduction in toxicity and an improvement in the drug's safety profile [3,4]. Moreover, nanocarriers can present superior therapeutic efficacy than free drugs due to the enhanced permeability and retention (EPR) effect, which allows the passive targeting and accumulation of nanostructures in the interstitial tissue of malignant tumors since they can pass through the leaky blood vessels [5,6].

Among the promising nanoplatforms for drug delivery in cancer therapy, nanostructured lipid carriers (NLC) have attracted expanding

* Corresponding author.
E-mail address: lucas@farmacia.ufmg.br (L.A.M. Ferreira).

https://doi.org/10.1016/j.biopha.2021.112373
Received 31 August 2021; Received in revised form 16 October 2021; Accepted 25 October 2021
Available online 28 October 2021

attention. They are composed of a blend of solid and liquid lipids that results in an unstructured system, which imparts many advantages over other lipid-based carriers, including enhanced physical stability, improved drug loading capacity, and flexible modulation of drug release [7,8].

In our previous report, we developed an NLC formulation for co-delivery of DOX, docosahexaenoic acid (DHA), and α-tocopherol succinate (TS) to cancer cells [9]. DHA is an omega-3 polyunsaturated fatty acid, and TS is a vitamin E derivative. Several studies have shown that these compounds can act as anticancer adjuvants, enhancing the antitumor activity of DOX and reducing its adverse effects [10–12]. Interestingly, both DHA and TS were used as functional excipients in that formulation: DHA is an oil that can form the lipid matrix of NLC and TS is an anionic counterion that can increase DOX encapsulation efficiency through hydrophobic ion-pairing [13].

In the present work, we conducted for the first time pharmacokinetic studies comparing DOX-TS ion-pair-loaded NLC and free DOX after intravenous administration in mice. The data obtained prompted us to synthesize DOX-TS covalent conjugates to be loaded into the NLC system. This strategy turned out to be interesting to increase the lipophilicity of DOX and enhance its retention in the lipid matrix of NLC.

Covalent conjugation of DOX and TS has been performed via amide or hydrazone bonds. Duhem et al. prepared an amide prodrug of DOX and TS that self-assembled into nanoparticles in the presence of TPGS [14]. Treatment with the formulation resulted in comparable efficacy to free DOX in CT-26 tumor-bearing mice, but with reduced toxicity. Recently, Xiong et al. also synthesized DOX-TS prodrugs through amide and hydrazone bonds and encapsulated them in TPGS micelles for drug co-delivery [15]. The amide-loaded micelles had low efficacy in inhibiting tumor growth in MCF-7 tumor-bearing mice, unlike the hydrazone-loaded formulation, which showed an antitumor activity comparable to free DOX. Furthermore, both conjugates-loaded formulations were able to reduce the toxic effects of DOX.

Based on the physiological differences between normal and tumor tissues, one attractive approach to improve the efficacy of chemotherapy is the development of nanocarriers with pH-triggered drug release. Typically, tumor tissues have lower extracellular pH values (pH ≈ 6.8) than normal tissues and the bloodstream, and moreover, endosomes and lysosomes inside cells exhibit much lower pH values (< 5.4) [16]. Thus, the use of acid unstable chemical bonds, such as amide, hydrazone, and imine, has attracted widespread interest [17,18]. DOX-loaded pH-sensitive nanocarriers have been shown to improve specific targeting to tumor tissues, enhance cell internalization, allow controlled drug release, and minimize potential damage to normal cells [15–19].

Herein, we report the synthesis of DOX-TS conjugates by either an amide (DOX-ami-TS) or a hydrazone (DOX-hyd-TS) bond. We performed in vitro studies to investigate their cytotoxicity in 4T1 breast cancer cells. We encapsulated the most active derivative in a DHA-based nanocarrier, characterized its physicochemical properties, investigated its pharmacokinetics and potential cardiotoxic effects in vivo. We also evaluated the antitumor efficacy and preliminary toxicity in a murine model of breast cancer.

2. Materials and methods

2.1. Materials

We obtained DOX·HCl from ACIC Chemicals (Ontario, Canada). We purchased α-tocopherol succinate (TS), ethylenediaminetetraacetic acid sodium (EDTA), 1-hydroxybenzotriazole (HOBt), 1-ethyl-3-(3-dimethylaminopropyl)carbodiimide hydrochloride (EDC), *N*-hydroxysulfosuccinimide (NHS), and *N,N*-dimethylformamide (DMF) from Sigma-Aldrich (St. Louis, USA). We obtained triethanolamine (TEA), triethylamine, glycerol, and hydrazine hydrate solution from Merck (Darmstadt, Germany). Compritol® 888 ATO (a mixture of mono-, di-, and triglycerides of behenic acid) was kindly provided by Gattefossé (Saint-Priest, France), and super-refined Polysorbate 80™ (Tween 80) and docosahexaenoic acid as triglyceride (OmeRx™ DHA 500TG) by Croda Inc. (Edison, USA). We purchased RPMI 1640 medium, fetal bovine serum, and trypsin-EDTA (0.25%) from Gibco-Invitrogen (Grand Island, USA). All other chemicals and reagents used in this study were of analytical grade.

2.2. Animals

In vivo experiments were conducted under the approval of the local Ethics Committee on Animal Use following the National Institutes of Health guide for the care and use of Laboratory Animals (Protocols #264/2018, #252/2020, #255/2020, and APAFiS#20238–201904 1116256696 v2). Healthy Swiss mice (male, 5–6 weeks old, 25–30 g) were used to assess the pharmacokinetics and short-term cardiotoxicity. To establish a murine model of breast cancer, we used BALB/c mice (female, 8-weeks old, 18–22 g) in the antitumor efficacy study. We kept the animals in an environment with a light cycle and controlled ventilation and allowed free access to food and water in all experiments.

2.3. Synthesis of DOX derivatives

DOX-TS conjugates were synthesized as previously described, with some modifications [14,15]. The synthesis routes are illustrated in Fig. 1. To prepare the amide derivative, we dissolved DOX·HCl (500 mg, 0.86 mmol) in 10 mL of warm DMF (55 °C) before the addition of triethylamine (200 μL, 1.43 mmol), HOBt (135 mg, 1.00 mmol), and TS (382 mg, 0.72 mmol). Then, EDC (192 mg, 1.00 mmol) dissolved in dichloromethane (30 mL) was added dropwise to the reaction mixture under stirring, and the solution was heated at 55 °C for 24 h. We transferred the reaction mixture to a separatory funnel, added diethyl ether (40 mL), and washed the mixture three times with 100 mL of brine. The organic phase was dried with Na_2SO_4, filtered, and evaporated using a vacuum rotary evaporator. DOX-ami-TS was collected as a red powder and dried in a vacuum (yield 662 mg, 87%, melting point range 102–105 °C).

To synthesize the hydrazone derivative, we dissolved TS (500 mg, 0.94 mmol), EDC (217 mg, 1.13 mmol), and NHS (130 mg, 1.13 mmol) in 2 mL of DMF, and stirred the solution overnight at room temperature. After that, hydrazine hydrate (100 μL, 2.04 mmol) was added to the reaction mixture, and the solution was further stirred for 20 min. We transferred the reaction mixture to a separatory funnel, added ethyl acetate (30 mL), and washed the mixture three times with 30 mL of 0.1 M HCl solution. The organic phase was dried with Na_2SO_4, filtered, and evaporated using a vacuum rotary evaporator. We immediately dissolved the hydrazide obtained (500 mg, 0.92 mmol) in 20 mL of methanol before adding DOX·HCl (178 mg, 0.31 mmol) and trifluoroacetic acid (25 μL, 0.33 mmol). After stirring overnight at room temperature, the solution was concentrated to approximately 5 mL using a vacuum rotary evaporator. Then, we added diethyl ether (35 mL) to precipitate the product, which was collected by centrifugation (16,800g, 15 min, 4 °C) and washed three times with water to remove the unreacted DOX. DOX-hyd-TS was collected as a red powder and dried in a vacuum (yield 238 mg, 72%, melting point range 157–160 °C).

The chemical identities of the conjugates were confirmed by the ^{1}H NMR spectra recorded on a Bruker AVANCE DRX400 instrument (Bruker, MA, USA) using tetramethylsilane as an internal standard. The ^{1}H NMR spectra are represented in Fig. 2 and are in accordance with previous published data [14,15]. ^{1}H NMR of DOX-ami-TS (400 MHz, $CDCl_3$): δ 8.01 (s, 1H), 7.97 (d, J = 5.4 Hz, 1H), 7.75 (t, J = 5.4 Hz, 1H), 7.35 (d, J = 5.4 Hz, 1H), 6.23 (bs, 1H), 5.47 (bs, 1H), 5.22 (bs, 1H), 4.77–4.76 (m, 2H), 4.18–4.12 (m, 2H), 4.04 (s, 3H), 3.65 (bs, 1H), 2.97–2.94 (m, 3H), 2.88–2.85 (m, 2H), 2.57–2.49 (m, 5H), 2.35–2.32 (m, 1H), 2.13 (dd, J = 9.7, 2.6 Hz, 1H), 2.03 (s, 3H), 1.93 (s, 3H), 1.89 (s, 3H), 1.84–1.81 (m, 2H), 1.55–1.48 (m, 4H), 1.39–1.33 (m, 4H), 1.28–1.25 (m, 6H), 1.19 (s, 3H), 1.15–1.10 (m, 3H), 1.09–1.03 (m, 5H),

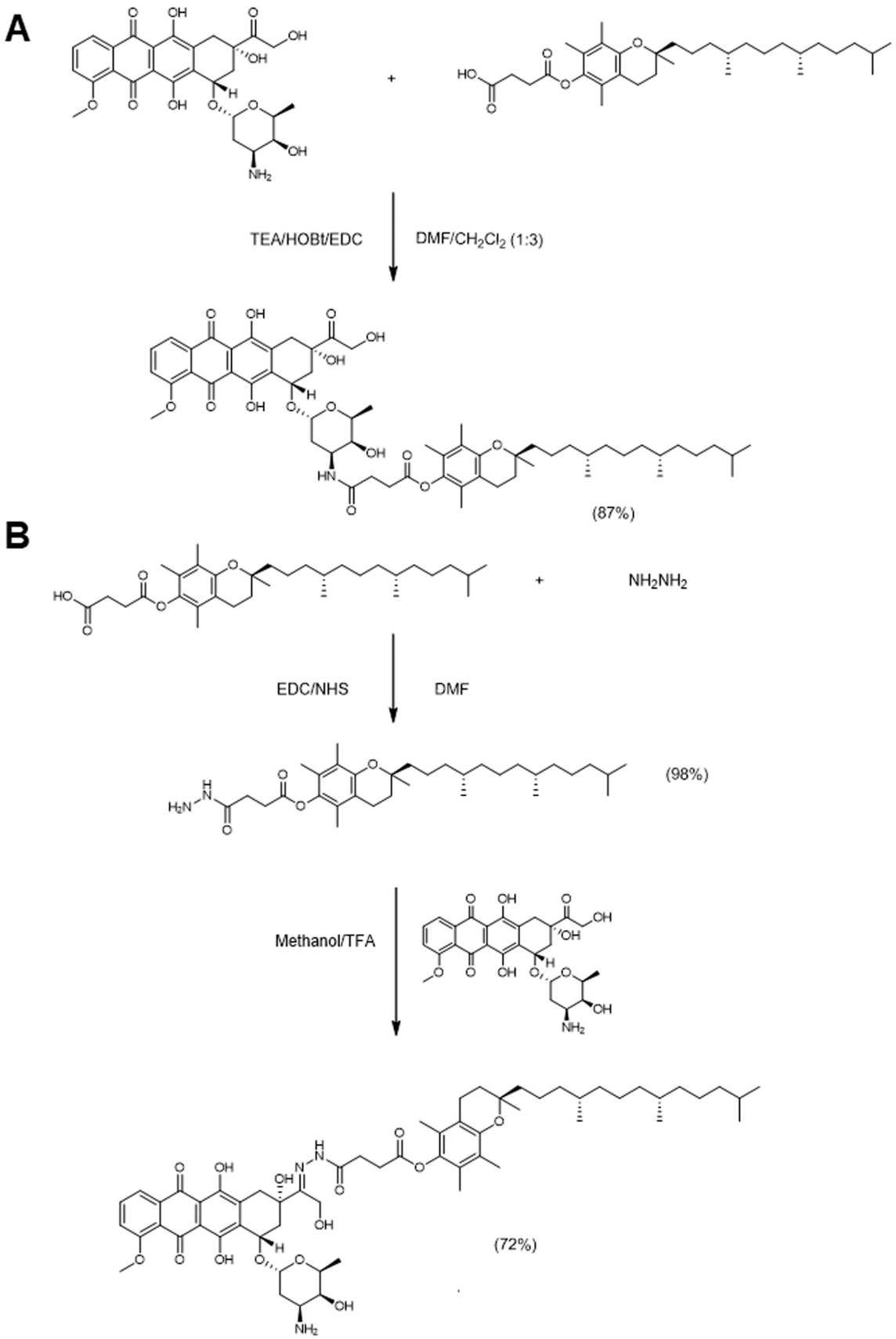

Fig. 1. Synthesis routes of DOX-ami-TS (A) and DOX-hyd-TS (B).

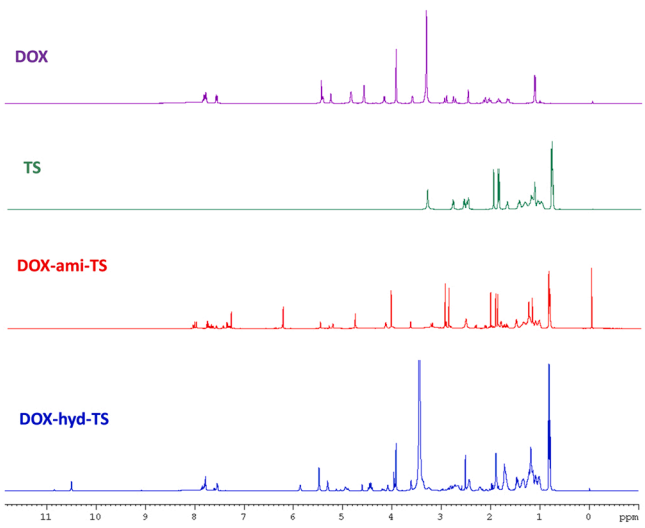

Fig. 2. Stacked ^{1}H NMR spectra of DOX, TS, DOX-ami-TS, and DOX-hyd-TS. DOX and DOX-hyd-TS were solubilized in DMSO-d6. TS and DOX-ami-TS were solubilized in $CDCl_3$.

0.88–0.82 (m, 15H). ^{1}H NMR of DOX-hyd-TS (400 MHz, DMSO-d6): δ 10.49 (s, 1H), 7.82–7.76 (m, 2H), 7.53 (d, $J = 5.2$ Hz, 1H), 5.85 (bs, 1H), 5.48 (bs, 2H), 5.30 (bs, 1H), 4.94 (bs, 1H), 4.48–4.38 (m, 2H), 4.09–4.06 (m, 1H), 3.91 (s, 3H), 3.68–3.58 (m, 1H), 3.60–3.20 (m, overlapped with the residual HOD signal of the solvent), 2.47–2.40 (m, 3H), 1.91–1.86 (m, 5H), 1.75–1.65 (m, 8H), 1.49–1.42 (m, 3H), 1.26–1.11 (m, 15H), 1.10–0.96 (m, 7H), 0.83–0.77 (m, 12H).

2.4. Cell culture and cytotoxicity assay

Murine 4T1 breast cancer cells were purchased from ATCC® (CRL-2539, American Type Culture Collection, USA). We grew and maintained cells in RPMI medium supplemented with FBS (10% v/v), penicillin (100 IU/mL), and streptomycin (100 µg/mL) in a 5% CO_2 atmosphere at 37 °C.

The in vitro cytotoxic effects of DOX and DOX-TS conjugates (DOX-ami-TS and DOX-hyd-TS) were assessed using the sulforhodamine B (SRB) assay as published elsewhere [20]. Briefly, 4T1 cells were seeded in 96-well plates (5×10^3 cells/well) 24 h before treatment. Then, we exposed the cells to a range of concentrations of DOX, DOX-ami-TS, and DOX-hyd-TS (DOX concentration range 0.08–10 µM; drug solutions were prepared by dissolving DOX in purified water and the conjugates in DMSO). After 48 h of incubation, 10% trichloroacetic acid (TCA) was added to each well to fix cells for one hour. Then, plates were washed with water to remove TCA and stained with SRB for 30 min, followed by a 1% acetic acid wash to remove unbound SRB. Then, we added 10 mM Tris-Base solution (pH 10.5) to solubilize the protein-bound dye, and the optical density was read at 510 nm using a microplate spectrophotometer Spectra Max Plus 384 (Molecular Devices, Sunnyvale, CA, USA). All experiments were performed in triplicate and IC_{50} values were calculated with GraphPad Prism® 6 software.

2.5. Preparation of NLC

DOX-TS ion-pair/NLC, in which DOX was encapsulated using the hydrophobic ion-pairing approach, was prepared and characterized as previously described [9]. In this work, after evaluating the cytotoxicity of the conjugates, we selected DOX-hyd-TS for further studies and encapsulated it in the NLC (DOX-hyd-TS/NLC). DHA was used in a triglyceride form (OmeRx™ DHA 500 TG) to compose the lipid matrix of the nanocarrier. The oily phase consisted of Compritol: 110 mg, DHA: 40 mg, Tween 80: 100 mg, TS: 40 mg, TEA: 6 mg, Glycerol: 220 mg, and DOX-hyd-TS: 20 mg; and the aqueous phase by EDTA: 4 mg and ultrapure water: 10 mL. We added glycerol to enhance the solubility of the hydrazone conjugate in the oil phase and prepared the formulation using the emulsification-ultrasound method (Fig. 3) as previously reported [9]. Blank-NLC was prepared similarly but in the absence of DOX-hyd-TS.

2.6. Characterization of NLC

2.6.1. Size distribution and shape

The mean particle size and zeta potential (ZP) were measured by dynamic light scattering (DLS) and DLS coupled with electrophoretic mobility, respectively, using Zetasizer Nano-ZS90 (Malvern Instruments, UK) with a fixed angle (90°) laser beam at 25 °C. We diluted the formulations 100 times in ultrapure water before the analyses. All experiments were performed in triplicate and data were reported as average size, polydispersity index (PDI), and ZP. Particle size distribution was also assessed by nanoparticle tracking analysis (NTA), carried out with a NanoSight NS300 (Malvern Instruments, UK). Data collection and analysis were performed using NTA 3.1 software. NLC was diluted 1×10^5 times in ultrapure water and introduced into the sample chamber with a disposable syringe. The analyses were made at room temperature for 60 s with automatic detection. All measurements were performed in triplicate. The morphology of nanocarriers was examined by cryogenic transmission electron microscopy (cryo-TEM). We prepared the samples by plunge freezing technique by spreading 3 µL of NLC into a thin film across a Formvar-copper grid and rapidly submerging it in liquid ethane. The vitrified samples were stored in liquid nitrogen during the analysis and observed using a transmission electron microscope (Tecnai G2–12, 120 kV, FEI, Hillsboro, USA).

2.6.2. Drug content and encapsulation efficiency (EE)

NLC was purified by filtration in a 0.45 µm polyvinylidene fluoride membrane to evaluate the encapsulation efficiency [21]. In this way, the entrapped drug passes freely through the membrane while the non-encapsulated remains precipitated in the filter. Briefly, samples of total NLC (before filtration) and purified NLC (after filtration) were dissolved first in THF and then in the mobile phase before injection in HPLC. We also determined the amount of drug soluble in the aqueous phase of the formulation using ultracentrifugal devices (Amicon® Ultra-4 100 kDa, Millipore, USA) [22], but the values were negligible since DOX-hyd-TS is highly hydrophobic. HPLC analyses were performed using an ACE C8 column (250 × 4.6 mm, 5 µm) and a mixture of 10 mM phosphate buffer pH 3: methanol (35:65) as the mobile phase with a flow rate of 1.0 mL/min. The injection volume was 20 µL and fluorescence detection was performed at ex/em wavelengths of 470/555 nm. %EE was calculated using the following equation: $\%EE = C_{AF}/C_T \times 100$; where: C_T = total concentration in NLC and C_{AF} = concentration after filtration of the NLC.

2.6.3. In vitro drug release

In vitro release studies were performed using the dialysis method under three different pH conditions (7.4, 6.8, and 5.0) [9,15]. Dialysis tubes with a cutoff size of 14 kDa (cellulose ester membrane; Sigma–Aldrich, St Louis, USA) were filled with 2 mL of NLC formulation, sealed, and incubated with 50 mL of release medium containing 1% Tween 80 (PBS pH 7.4 and 6.8; isotonic acetate buffer pH 5.0). The samples were kept under magnetic stirring at 250 rpm and 37 °C. We withdrew aliquots of 0.5 mL at several time points and determined drug concentrations by HPLC as described above. The release medium was completed with the same volume after each sample collection. The values were plotted as the cumulative percentage of DOX released.

2.6.4. Preliminary evaluation of stability

The formulations (n = 3 batches) were kept in amber borosilicate glass bottles within a nitrogen atmosphere and stored at 4 °C. At 15 and

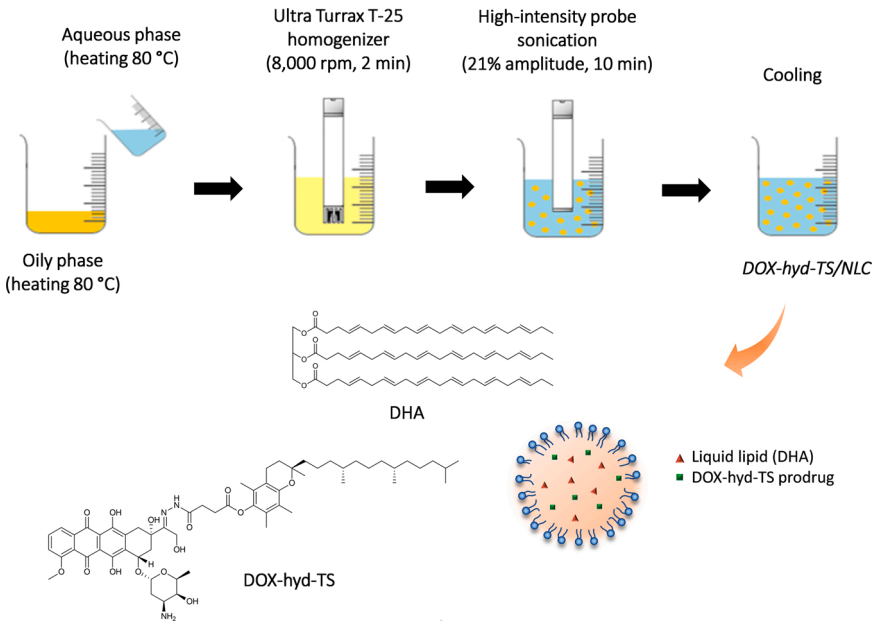

Fig. 3. Schematic illustration of DOX-hyd-TS/NLC preparation using the emulsification-ultrasound method. Briefly, the heated oily and aqueous phases were mixed under constant agitation with an Ultra Turrax T-25 homogenizer. The formed emulsion was immediately submitted to a high-intensity probe sonication and cooled down to room temperature with manual agitation to produce the NLC.

30 days after preparation, aliquots of the samples were analyzed for particle size, PDI, ZP, and EE. The mean values for each parameter were compared with those obtained at the time of preparation (day 0).

2.7. Pharmacokinetics

We randomly divided Swiss mice into three groups (n = 4 mice per group): free DOX, DOX-hyd-TS/NLC, and DOX-TS ion-pair/NLC. Non-encapsulated DOX-hyd-TS was not used in the in vivo experiments since this conjugate is highly hydrophobic, and solubilizers such as Chemophor or DMSO have been associated with toxicity issues [23]. Briefly, the animals received a single dose equivalent to 5 mg/kg of DOX via the tail vein. At 5 min, 0.5 h, 1 h, 2 h, 4 h, and 24 h post-injection, the animals were anesthetized with a mixture of ketamine (80 mg/kg) and xylazine (15 mg/kg), and blood was collected by puncture of the brachial plexus in tubes containing an anticoagulant (0.1% w/v EDTA). After centrifugation at 1400g for 10 min, an aliquot of 125 μL of the supernatant plasma was collected and fortified with 25 μL of a daunorubicin solution (internal standard, 400 μg/mL in acetonitrile). Then, the samples were mixed with 150 μL of 0.1% perchloric acid in acetonitrile to precipitate the proteins. After centrifugation at 9400g for 15 min, the supernatants were collected and injected in HPLC to determine DOX concentrations. Standard calibration curves were prepared using plasma from untreated mice. The pharmacokinetic parameters were calculated by the PKSolver software using non-compartmental analyses and the linear trapezoidal method [24].

2.8. Short-term cardiotoxic effects

We randomly divided Swiss mice into three groups (n = 10 mice per group): blank-NLC, DOX-hyd-TS/NLC, and free DOX. The animals were injected through the tail vein with repeated doses equivalent to 5 mg/kg/day of DOX. The injections were performed every two days, in a total of five administrations, reaching a cumulative dose of 25 mg/kg. We assessed cardiac function and electrophysiology before treatment (baseline) and two days after the last administration by electrocardiogram (ECG) and echocardiogram analyses. ECG was continuously recorded during 10 min under anesthesia (1–2% isoflurane inhalation) using two limb leads and monitored with a Power Lab system (LabChart v7, AD Instruments, Australia). Beat rate and PR, QRS, and QT intervals were measured from the ECG signal. We performed high-resolution echocardiography on a Vevo 3100 system (Fujifilm VisualSonics, Canada) equipped with an MX550D 40 MHz ultrasound probe. Data were acquired under anesthesia (1–2% isoflurane inhalation) and monitoring of body temperature, ECG, and respiration [25]. Morphological and functional cardiac parameters were characterized in the M-mode from a short-axis view. We also recorded the mitral inflow by pulsed-wave Doppler in an apical four-chamber view [26]. Offline image analyses were performed using dedicated Visual Sonics Vevo 3100 3.1.0 software.

2.9. Evaluation of antitumor activity

Cultured 4T1 cells (1.0×10^6 cells in 100 μL PBS) were collected and injected subcutaneously into the right thigh of BALB/c mice to establish the tumor-bearing mouse model. When tumor volume reached approximately 150 mm^3, we randomly divided the animals into four groups (n = 6 mice per group): blank-NLC, DOX-hyd-TS/NLC, free DOX, and Lip-DOX (pegylated liposomal DOX). Lip-DOX is similar to commercial Doxil® in size, lipid composition, and the amount of encapsulated drug and was prepared as described elsewhere [27]. The animals were injected through the tail vein with repeated doses equivalent to 5 mg/kg/day of DOX. The injections were performed every two days, in a total of five administrations, reaching a cumulative dose of 25 mg/kg. The antitumor efficacy was determined by measuring the tumor volume with a fine caliper (Mitutoyo, MIP/E-103) every two days, from the first day of treatment until two days after the last administration [9].

2.10. Toxicity evaluation

During the assessment of antitumor efficacy, we evaluated behavioral/clinical modifications, body weight, and mice mortality. On the last day of the study, blood was collected from anesthetized mice by puncturing the brachial plexus. We performed hematologic and biochemical analyses as described elsewhere [27]. After blood collection, the animals were euthanized and the heart, lungs, spleen, liver, kidneys, and tumor were removed for histopathological examination [9].

2.11. Data analysis

Statistical analyses were performed using GraphPad Prism software (version 6.00, La Jolla, California, USA). We tested the difference between the experimental groups by Student's *t*-test or one-way ANOVA followed by Tukey's test. Survival curves were analyzed by the Log-rank (Mantel-Cox) test. For all analyses, a 95% confidence interval was adopted, and differences were considered significant when the p-value was less than 0.05 ($p < 0.05$).

3. Results

3.1. Cytotoxicity assay

We investigated the cytotoxicity of DOX derivatives in 4T1 breast cancer cells after 48 h of incubation. DMSO used to solubilize the compounds did not affect cell viability and showed similar results to non-treated cells (data not shown). As shown in Fig. 4A, DOX-ami-TS exhibited low cytotoxicity, with cell viability above 60% even at the highest concentration. Consequently, we were not able to calculate the IC_{50} value for the amide derivative. On the other hand, DOX-hyd-TS effectively inhibited the proliferation of tumor cells (IC_{50} value: 0.32 ± 0.10 μM). This conjugate exhibited cytotoxicity comparable to DOX (IC_{50} value: 0.15 ± 0.02 μM) and higher than DOX-ami-TS. Therefore, we selected DOX-hyd-TS for further studies due to its more significant cytotoxic effect against tumor cells.

3.2. NLC characterization

We prepared NLC formulations with and without DOX-hyd-TS by the hot melting homogenization method. Table 1 presents the physicochemical data. Both blank-NLC and DOX-hyd-TS/NLC showed an average size close to 90 nm with narrow size distribution (PDI < 0.30), suggesting monodisperse systems. The zeta potential was highly negative, probably due to the free TS used in the NLC composition, which is ionized on the particle surface. The addition of DOX-hyd-TS did not increase the particle size, indicating that the lipid matrix could properly incorporate the hydrophobic derivative. The encapsulation rate near 100% confirmed the effective entrapment of the conjugate in the nanocarrier. These characterization data were similar to those reported for DOX-TS ion-pair/NLC [9]. We also evaluated nanoparticle size distribution by NTA (Table S1). The average diameter measured by NTA was similar to that determined by DLS. In addition, the size distribution profile (approximately 90% < 140 nm, 50% < 90 nm, 10% < 70 nm) confirmed the narrow distribution (Fig. 4B) as observed before. Morphological analyses of the NLC were performed by cryo-TEM and a representative image for DOX-hyd-TS/NLC is shown in Fig. 4C. The particles generally showed reasonably uniform diameters, with spherical morphology, smooth surface, and visible boundary. These results confirmed a single population of particles as previously demonstrated by DLS and NTA. In the short-term stability test, no significant variation in the parameters was observed, indicating no loss of formulation stability (Fig. S1). These results suggest no aggregation or fusion phenomena that could alter the average diameter and unwanted release of the encapsulated DOX.

We investigated the in vitro drug release at 37 °C under different pH conditions (7.4, 6.8, and 5.0). These conditions correspond to the normal physiological pH, the tumor microenvironment, and the endosomal compartments of tumor cells, respectively [9,15]. As shown in Fig. 4D, around 16% of DOX was released from DOX-hyd-TS/NLC after 24 h at pH 7.4, reaching only 22% in 48 h. We observed a more pronounced drug release at pH 6.8, with 41% of DOX released within 48 h. In turn, at pH 5.0, a release of 62% of DOX occurred within 24 h and approximately 85% up to 48 h. Therefore, DOX was released from the NLC in a controlled and significantly pH-dependent manner ($p < 0.05$).

3.3. Pharmacokinetics

Pharmacokinetic studies were performed in mice after a single intravenous administration of free DOX, DOX-hyd-TS/NLC, and DOX-TS ion-pair/NLC. Fig. 4E and Table 2 show, respectively, the plasma concentration-time profiles and the major pharmacokinetic parameters. We found comparable in vivo behavior for free DOX and DOX-TS ion-pair/NLC, with virtually identical pharmacokinetic parameters. These data suggest that DOX encapsulated by the ion-pairing approach was quickly released from the NLC after administration to the animals, exhibiting behavior similar to the free drug. On the other hand, a significant improvement in pharmacokinetics was achieved when DOX was encapsulated as a hydrophobic conjugate with TS. Higher plasma concentrations were observed for DOX-hyd-TS/NLC throughout the study. Noteworthy, we found an 8-fold increase in plasma concentration at 5 min compared to free DOX and DOX-TS ion-pair/NLC. Furthermore, the plasma kinetics of DOX-hyd-TS/NLC showed significantly higher AUC and C_{max}, lower clearance rate, and lower volume of distribution compared to the other groups. Therefore, we conducted further in vivo studies using DOX-hyd-TS/NLC, as the pharmacokinetics of DOX-TS ion-pair/NLC was comparable to that of the free drug.

3.4. Evaluation of cardiotoxic effects

We recorded ECG signals before and after the animals received the fifth treatment dose of blank-NLC, DOX-hyd-TS/NLC, and free DOX. No significant changes in heart rate, PR, and QRS intervals were found compared to the baseline for all treatment groups (Fig. 5). In turn, significant prolongation in the QT interval at the end of treatment was observed in animals receiving free DOX, which did not occur for the blank-NLC and DOX-hyd-TS/NLC groups. Fig. 6 shows echocardiographic analyses. The left ventricular ejection fraction, fractional shortening, and cardiac output of mice treated with nanoformulations did not show any changes compared to the baseline. In contrast, animals repeatedly administered free DOX displayed impaired left ventricular systolic function two days after the end of treatment, reflected in reduced ejection fraction, fractional shortening, and cardiac output. No deaths occurred precisely during this study, but 70% of the animals treated with free DOX died a few days later, hampering the investigation of late cardiotoxicity. On the other hand, the survival of all animals was verified in the other groups, even some time later. We also determined the E/A ratio by pulsed-wave Doppler as an index of left ventricular diastolic function. Similar values at the study's beginning and end were found for all groups, indicating that the treatments did not compromise diastolic function.

3.5. In vivo antitumor efficacy

The antitumor activity was investigated by measuring tumor volume every other day in 4T1 tumor-bearing mice treated with blank-NLC, DOX-hyd-TS/NLC, free DOX, and Lip-DOX. As shown in Fig. 7A, rapid tumor growth was observed in the animals from the control group, given the aggressiveness and high rate of cell proliferation of the 4T1 cell line. In contrast, we observed slower tumor growth in the other groups that received formulations containing DOX. Treatment with DOX-hyd-TS/NLC was the most effective in controlling tumor progression since the animals that received this formulation had the smallest tumor volumes at the end of the study. Indeed, a higher tumor inhibition ratio was achieved after treatment with DOX-hyd-TS/NLC (61%) compared to free DOX (44%) and Lip-DOX (56%).

Fig. S2 shows histological sections of tumor tissue evaluated after treatment. Mice that received blank-NLC showed tumors with ulceration, a central area of necrosis, and vast regions of viable cells with mitotic figures, indicating a high rate of cell proliferation. In contrast, all other groups had smaller tumors and larger necrosis areas due to DOX-induced cell death compared to the control group.

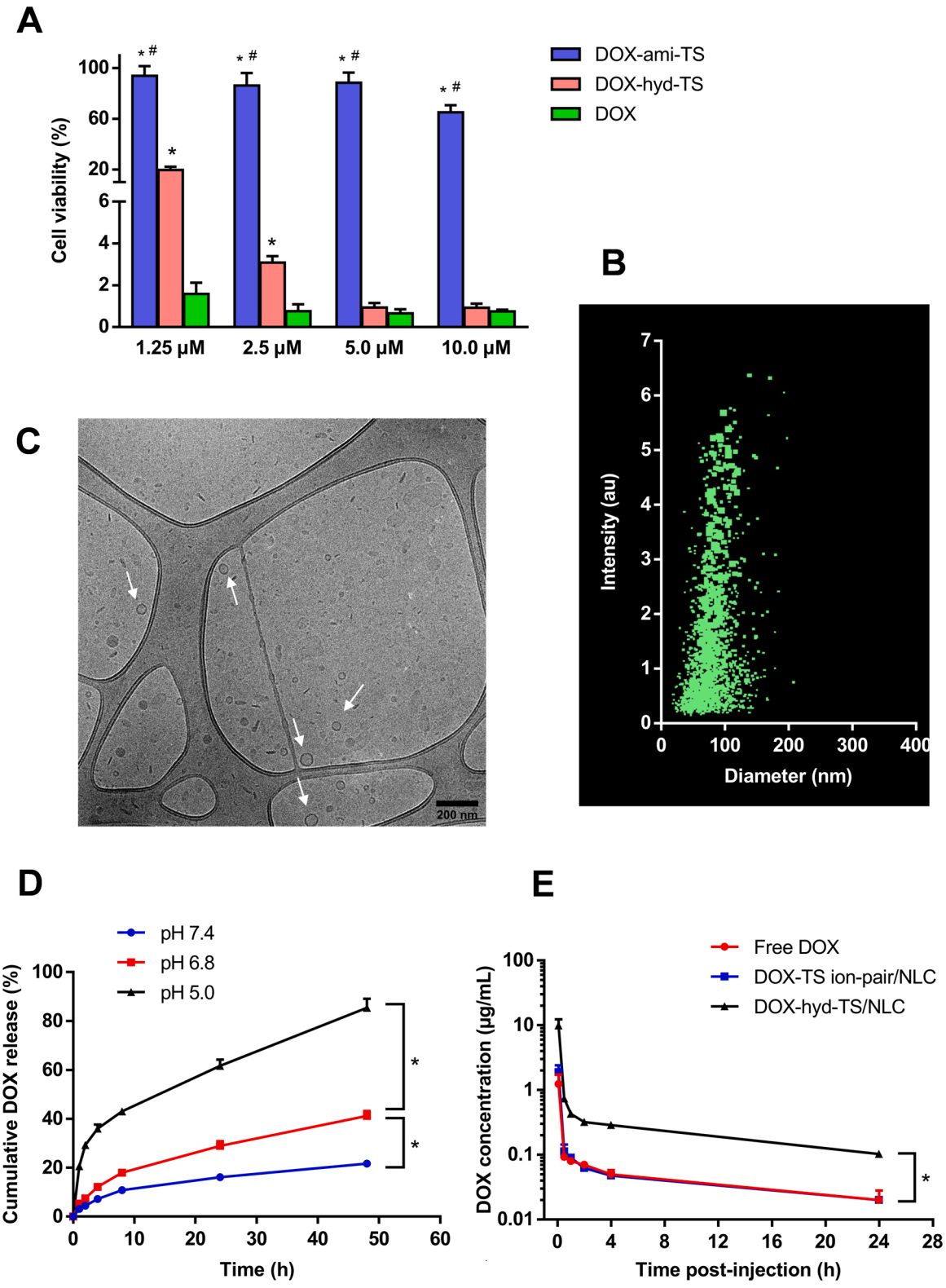

Fig. 4. (A) *In vitro* cytotoxicity of DOX, DOX-ami-TS, and DOX-hyd-TS in 4T1 breast cancer cells (data represented as mean ± SD, n = 3, * and # Represents a significant difference compared to DOX and DOX-hyd-TS, respectively ($p < 0.05$)). (B) Plot of particle size distribution x intensity for DOX-hyd-TS/NLC measured by nanoparticle tracking analysis. (C) Cryo-TEM image of DOX-hyd-TS/NLC. White arrows indicate nanostructures. (D) *In vitro* release studies of DOX-hyd-TS/NLC performed in different pH conditions (pH 5.0, 6.8, and 7.4), at 37 °C, by the dialysis method (data represented as mean ± SD, n = 3, * Represents significant differences between the groups ($p < 0.05$)). (E) Semi-logarithmic plasma concentration-time curves after intravenous administration of DOX solution, DOX-TS ion-pair/NLC, or DOX-hyd-TS/NLC in Swiss mice at a dose of 5 mg/kg (data represented as mean ± SEM, n = 4, * Represents significant differences between the groups ($p < 0.05$)).

Table 1
Physicochemical characterization of blank-NLC and DOX-hyd-TS/NLC.

Parameters	blank-NLC	DOX-hyd-TS/NLC
Mean size (nm)	84 ± 2	91 ± 2
PDI	0.22 ± 0.01	0.25 ± 0.02
Zeta potential (mV)	- 43 ± 2	- 39 ± 2
EE (%)	–	99 ± 1

Note: Results expressed as mean ± SD (n = 3). PDI: polydispersity index; EE: encapsulation efficiency.

Table 2
Pharmacokinetic parameters of DOX solution and NLC formulations. Each treatment was intravenously administered in mice at a dose of 5 mg/kg of DOX.

Parameters	Groups		
	Free DOX	DOX-TS ion-pair/ NLC	DOX-hyd-TS/ NLC
C_{max} (μg/mL)	1.23 ± 0.25	1.88 ± 0.26	9.90 ± 1.23[a]
$t_{1/2}$ (h)	12.7 ± 1.6	11.9 ± 0.6	13.9 ± 1.4
AUC_{0-t} (μg/mL*h)	1.32 ± 0.12	1.51 ± 0.12	8.49 ± 0.52[a]
$AUC_{0\text{-}inf}$ (μg/ mL*h)	1.69 ± 0.19	1.79 ± 0.12	10.59 ± 0.32[a]
$MRT_{0\text{-}inf}$ (h)	13.2 ± 2.2	10.1 ± 0.8	12.7 ± 1.9
Cl (L/h)	0.092 ± 0.009	0.085 ± 0.005	0.014 ± 0.001[a]
V_z (L)	1.64 ± 0.15	1.46 ± 0.13	0.29 ± 0.03[a]

Note: Results expressed as mean ± SEM (n = 4). C_{max}: maximum concentration in plasma; $t_{1/2}$: elimination half-life; AUC: area under the concentration-time curve; MRT: mean residence time; Cl: clearance; V_z: apparent volume of distribution during the terminal phase.
[a] Represents a significant difference compared to free DOX and DOX-TS ion-pair/NLC ($p < 0.05$).

3.6. Preliminary toxicity evaluation

We monitored mice's body weight every two days throughout the study and the results are shown in Fig. 7B. Weight gain was observed only in the animals treated with blank-NLC, evidencing the safety of blank-formulation. Weight loss was significantly lower in the animals treated with DOX-hyd-TS/NLC than free DOX and Lip-DOX. As shown in Fig. 7C, pronounced clinical signs of toxicity, such as prostration and intense piloerection, were observed in animals from the free DOX group, while no or few alterations were found in mice treated with nano-formulations (data shown for DOX-hyd-TS/NLC). In fact, only in the free DOX group did the death of mice occur from the seventh day after the beginning of the study, corresponding to the fourth injected dose (Fig. 7D).

3.7. Hematologic analyses

Hematologic analyses were performed at the end of treatment and results are summarized in Table 3. We found alterations in some parameters compared to the reference values [28] in all groups due to the 4T1 breast cancer, which induces a severe leukemoid reaction and an anemic phenotype in mice with low red blood cell count, platelets, hematocrit, and hemoglobin levels [29]. The animals that received blank-NLC showed a significant increase in the number of white blood cells due to the rapid tumor growth, while this was not observed in the other groups. Treatment with all formulations containing DOX led to a reduction in platelet count, indicating a certain level of DOX-induced bone marrow toxicity. However, this reduction was significantly lower for mice treated with DOX-hyd-TS/NLC than those who received free DOX. Red blood cells count, hemoglobin, hematocrit, and RDW were similar in all treatment groups. (Table 4).

3.8. Biochemical analyses

Biochemical analyses were also performed in order to investigate renal, hepatic, and cardiac toxicity. Both urea and creatinine were similar in all groups, indicating no renal toxicity. As an indicator of DOX-induced hepatic injury, mice treated with free DOX showed a significant increase in ALT and AST levels compared to those treated with blank-NLC. Were also found increased AST levels in animals that received Lip-DOX. In contrast, mice treated with DOX-hyd-TS/NLC showed ALT and AST levels similar to the control group. Concerning cardiac toxicity, treatment with free DOX resulted in significantly higher levels of CK-MB, while animals that received Lip-DOX and DOX-hyd-TS/NLC showed values similar to those in the control group.

3.9. Histopathological examination

After treatment, histopathologic analyses were carried out on mice's kidneys, spleen, lungs, liver, and heart. In agreement with the biochemical results, all groups showed preserved renal tissues with their typical architecture. We observed an enlarged spleen in animals that received blank-NLC, consistent with the leukemoid reaction and splenomegaly caused by the 4T1 tumor. In contrast, mice from the other groups showed normal-sized spleens, indicating that the treatments could overcome splenomegaly. We found pulmonary metastases in all groups due to the 4T1 breast tumor (Fig. S3), which is highly tumorigenic, invasive, and spontaneously metastasizing to distant organs [29]. However, while most mice treated with blank-NLC had extensive and numerous metastatic foci in the lungs, in the other groups, only a few animals presented small and localized metastases, indicating that DOX therapy reduced the potential for tumor invasiveness.

We also evidenced multiple metastatic foci in the liver of mice receiving blank-NLC (Fig. 8A). In contrast, animals in the other groups did not show metastatic foci, and only mild hydropic degeneration and rare inflammatory cell infiltration were found, especially for those treated with Lip-DOX and DOX-hyd-TS/NLC, possibly due to the high uptake of these particles by the liver [30]. Regarding the histologic evaluation of the heart, mice treated with blank-NLC revealed cardiac tissue with typical architecture and cardiac fibers of the usual thickness (Fig. 9). In contrast, we detected large areas of cardiomyocyte vacuolization and hyaline degeneration in animals treated with free DOX. Mice that received Lip-DOX and DOX-hyd-TS/NLC showed fewer vacuoles and mild hyalinization, indicating better protection against the cardiotoxic effects of DOX.

4. Discussion

Hydrophobic ion-pairing has emerged as a method to modulate the solubility of hydrophilic charged molecules and improve their incorporation into several delivery nanocarriers, such as lipid nanoparticles, nanoemulsions, and polymeric micelles [13,22,31]. Recently, our group used this approach to develop an NLC system encapsulating DOX with the anticancer adjuvants DHA and TS [9]. We achieved high DOX encapsulation efficiency due to ion-pairing with TS. Our data confirmed the therapeutic potential of this new formulation, given its high antitumor activity in vivo and lower toxicity than those observed for free DOX due to the synergistic effect of the drugs. However, pharmacokinetic studies had not been performed, and this has been one of the critical challenges associated with the ion-pairing approach [32,33].

In the present work, we extended our studies by evaluating the pharmacokinetics after intravenous administration in mice. The data obtained indicated pharmacokinetics virtually equal to free DOX, suggesting a rapid destabilization of the ion-pair and the consequent release of DOX from the NLC after administration to the animals. Li et al. reported a similar behavior for polymeric nanoparticles encapsulating DOX and hyaluronic acid via electrostatic interactions, which showed a significant burst effect in the plasma after intravenous injection [33].

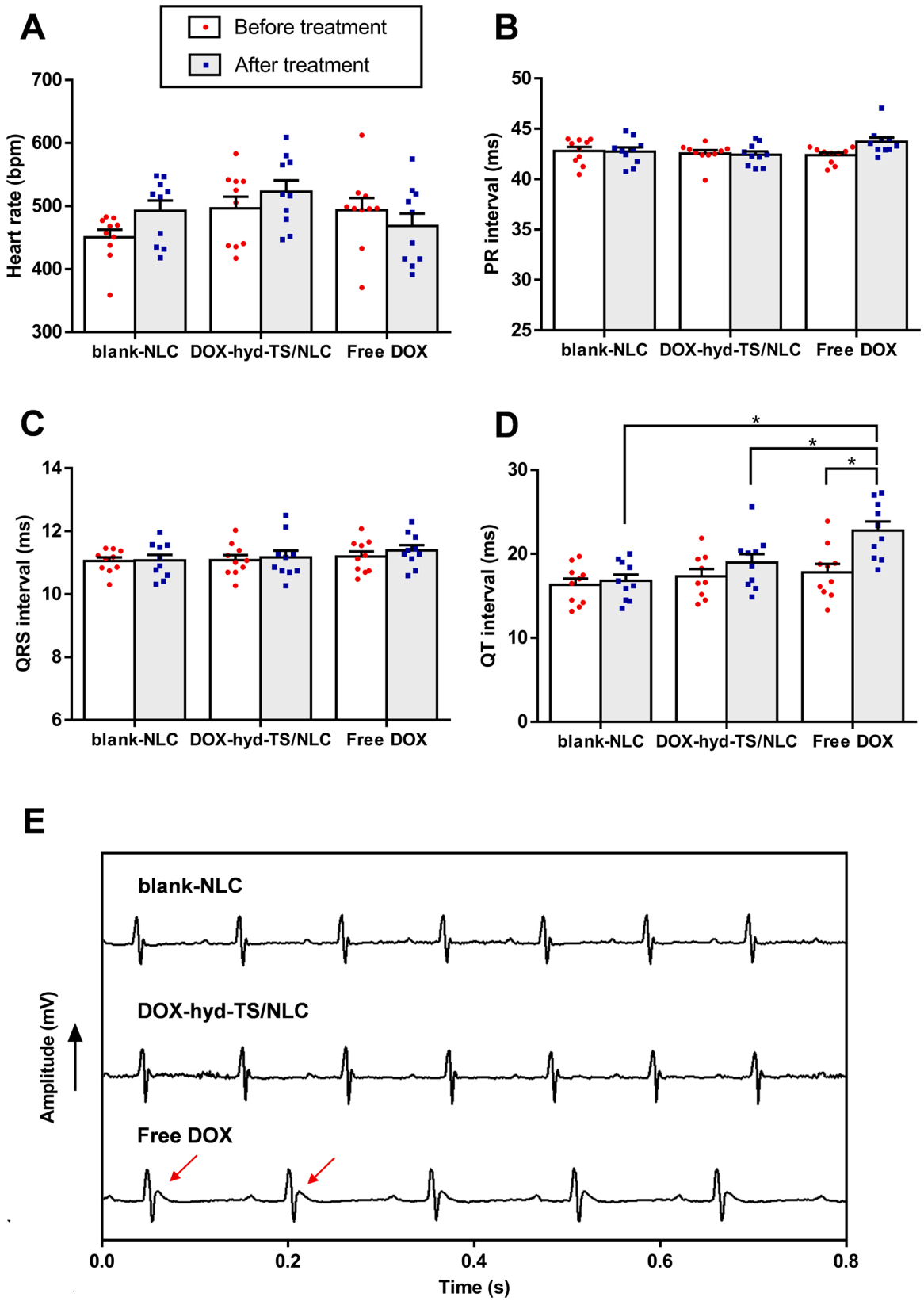

Fig. 5. (A-D) ECG parameters measured in Swiss mice before and after repeated administration of DOX solution, blank-NLC, and DOX-hyd-TS/NLC. (E) Representative ECG signals recorded at the end of the experiment showing QT prolongation for the free DOX group (red arrows). Each treatment was intravenously administered five times, every two days, at 5 mg/kg (data represented as individual values and mean ± SEM, n = 10). * Represents significant differences between the groups ($p < 0.05$).

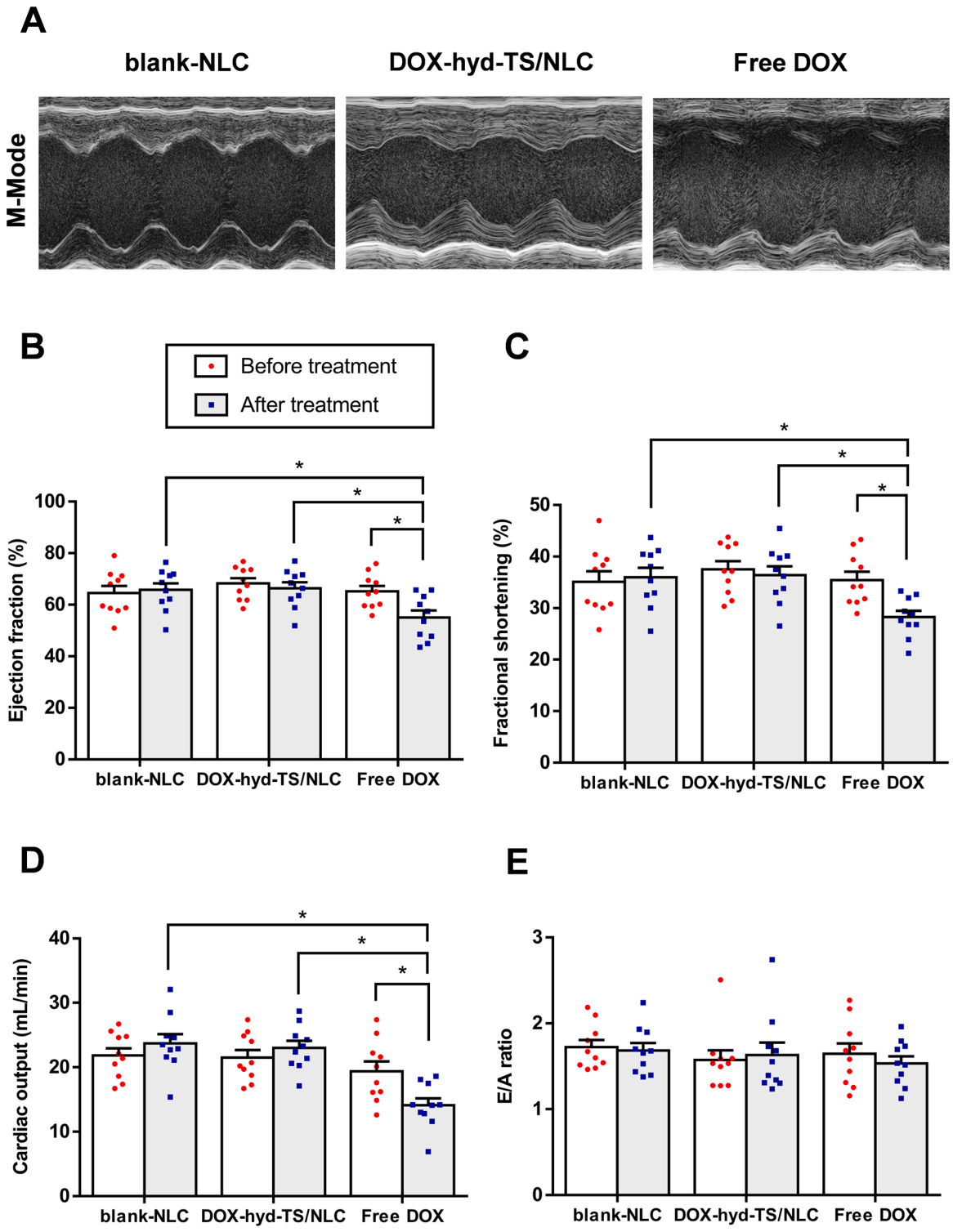

Fig. 6. Echocardiographic parameters measured in Swiss mice before and after repeated administration of DOX solution, blank-NLC, and DOX-hyd-TS/NLC. (A) Representative M-mode echocardiography parasternal short-axis view recorded at the end of the experiment, (B) Left ventricular ejection fraction, (C) Fractional shortening, (D) Cardiac output, and (E) E/A ratio. Each treatment was intravenously administered five times, every two days, at a 5 mg/kg (data represented as individual values and mean ± SEM, n = 10). * Represents significant differences between the groups ($p < 0.05$).

Considering that one of the nanomedicine principles is to improve the pharmacokinetics of encapsulated drugs, the results obtained with DOX-TS ion-pair/NLC were not satisfactory, making us give up on this approach.

To overcome this drawback, we proposed the synthesis of DOX-TS hydrophobic conjugates to improve the retention of DOX in the lipid nanocarrier. TS is a succinic acid ester of vitamin E and one of the most effective anticancer compounds in the vitamin E family. It can enhance the efficacy of conventional anticancer drugs and protect normal cells from chemotherapy-induced toxicity by multiple pathways [12,34,35]. Several anticancer prodrugs were obtained in recent years by conjugating TS with cytotoxic drugs, such as paclitaxel, camptothecin, and

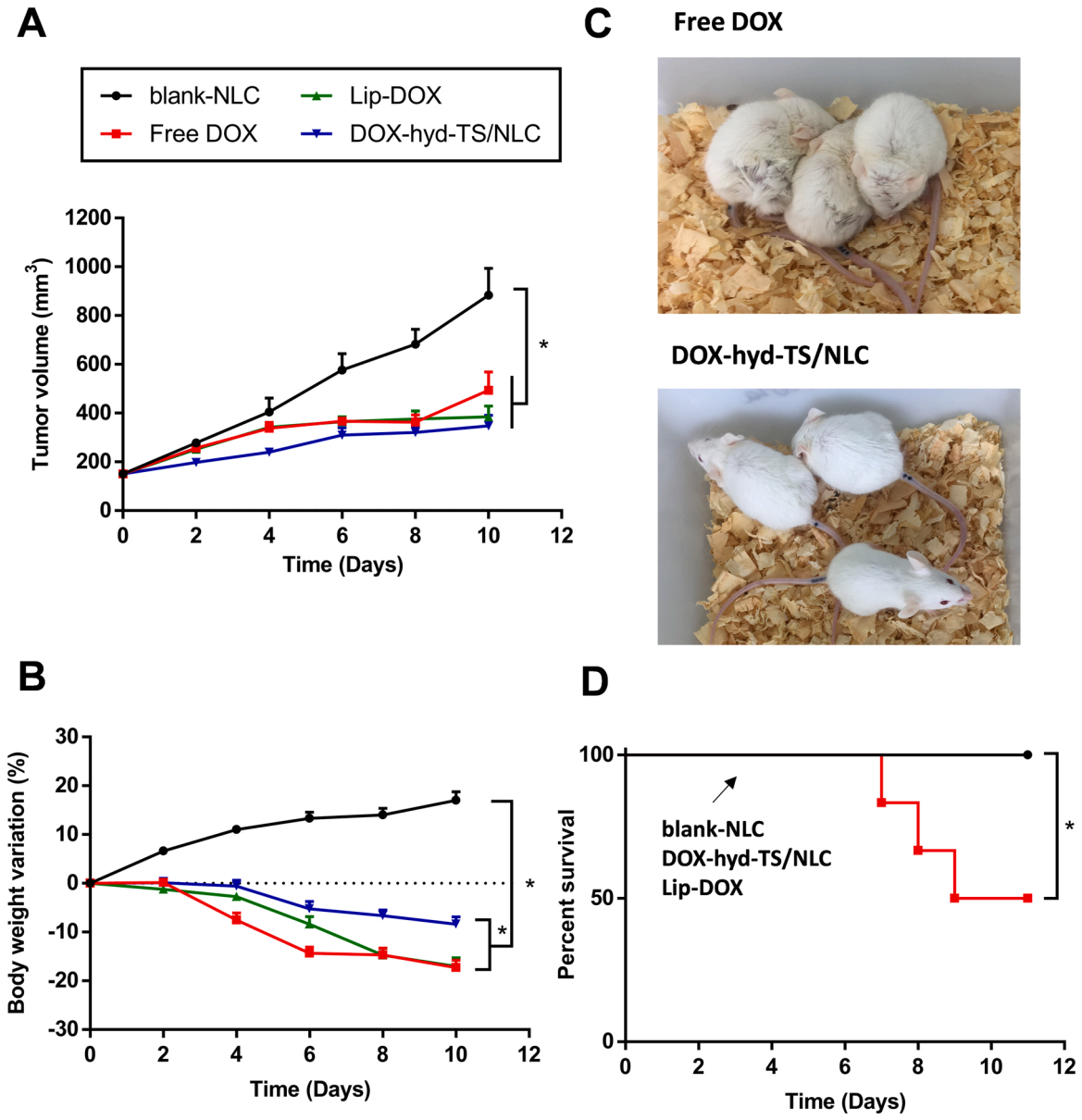

Fig. 7. (A) In vivo therapeutic efficacy of DOX solution, blank-NLC, DOX-hyd-TS/NLC, and Lip-DOX in 4T1 tumor-bearing BALB/c mice. (B) Percentage of body weight variation during the experiment. (C) Representative images of mice treated with free DOX and DOX-hyd-TS/NLC showing clinical signs of toxicity for the free DOX group. (D) Kaplan-Meier survival curves in the different groups. We plotted Blank-NLC, DOX-hyd-TS/NLC, and Lip-DOX curves together because we observed no deaths in these groups. Each treatment was intravenously administered five times, every two days, at a 5 mg/kg (data represented as mean ± SEM, n = 6). * Represents significant differences between the groups ($p < 0.05$).

Table 3
Hematologic parameters of 4T1 tumor-bearing BALB/c mice after different treatments. Each treatment was intravenously administered five times, every two days, at a dose of 5 mg/kg of DOX.

Parameters	Reference values[28]	Groups			
		blank-NLC	Free DOX	Lip-DOX	DOX-hyd-TS/NLC
White blood cells (10^9/L)	2–10	56.2 ± 6.9	3.7 ± 0.8[a]	5.3 ± 1.0[a]	5.9 ± 1.4[a]
Red blood cells (10^{12}/L)	7–11	5.9 ± 0.4	4.3 ± 0.3	5.1 ± 0.2	4.7 ± 0.2
Hemoglobin (g/L)	13–18	9.9 ± 1.1	7.8 ± 0.6	9.8 ± 0.5	8.7 ± 0.4
Hematocrit (%)	40–50	28.0 ± 2.4	19.8 ± 1.4	23.8 ± 0.9	21.7 ± 0.8
RDW (%)	11–15	14.6 ± 0.2	13.3 ± 0.1	13.9 ± 0.1	13.9 ± 0.1
Platelets (10^9/L)	1000–2000	387 ± 39	199 ± 16[a]	244 ± 28[a]	264 ± 23[a,b]

Note: Results expressed as mean ± SEM (n = 6). RDW: red cell distribution width.
[a] Represents a significant difference compared to blank-NLC.
[b] Represents a significant difference compared to free DOX ($p < 0.05$).

Table 4
Biochemical parameters of 4T1 tumor-bearing BALB/c mice after different treatments. Each treatment was intravenously administered five times, every two days, at a dose of 5 mg/kg of DOX.

Parameters	Groups			
	blank-NLC	Free DOX	Lip-DOX	DOX-hyd-TS/ NLC
Creatinine (mg/dL)	0.38 ± 0.03	0.28 ± 0.03	0.25 ± 0.02	0.28 ± 0.01
Urea (mg/ dL)	62.4 ± 6.4	109.7 ± 12.8	75.7 ± 11.7	64.5 ± 4.1
ALT (U/L)	29.0 ± 2.2	141.4 ± 31.1[a]	75.8 ± 8.0	52.8 ± 3.7[b]
AST (U/L)	114.6 ± 12.2	298.6 ± 40.6[a]	252.6 ± 32.4[a]	154.6 ± 13.6[b,c]
CK-MB (U/ L)	40.1 ± 4.7	194.1 ± 49.2[a]	72.9 ± 17.7[b]	49.3 ± 3.2[b]

Note: Results expressed as mean ± SEM (n = 6). ALT: alanine aminotransferase; AST: aspartate aminotransferase; CK-MB: creatine kinase-myocardial band.
[a] Represents a significant difference compared to blank-NLC.
[b] Represents a significant difference compared to free DOX.
[c] Represents a significant difference compared to Lip-DOX ($p < 0.05$).

DOX [14,15,36,37].

In this study, we synthesized amide and hydrazone prodrugs of DOX and TS according to the procedures previously described, with some modifications [14,15]. The conjugates were obtained without laborious purification methods and with good yields, above 70% for both. The amide derivative showed low cytotoxic effects to kill 4T1 breast cancer cells, which was later confirmed in preliminary studies using 4T1 tumor-bearing mice (data not shown). This behavior can probably be explained by the intracellular stability of the conjugate, which did not release a substantial amount of DOX. Previous studies have shown that some amide bonds can be very chemically stable, even in biological environments [38,39]. On the other hand, the hydrazone conjugate effectively decreased cell viability, presenting an antitumor activity comparable to DOX in some tested concentrations. However, this conjugate had a higher IC_{50} value, resulting from an incomplete or delayed in vitro conversion of the conjugate to release DOX and TS.

To investigate the in vivo therapeutic potential of DOX-hyd-TS, we encapsulated it in a DHA-based nanocarrier. DHA is an omega-3 fatty acid that can enhance the cytotoxic activity of anticancer drugs, primarily by increasing the sensitivity of cancer cells and producing oxidative damage species [10,40]. In addition, cardioprotective effects have been attributed to it, which can be extremely useful when used in combination therapy with DOX [11,41,42]. Both blank-NLC and DOX-hyd-TS/NLC showed mean diameters close to 90 nm and uniform size distribution determined by DLS and NTA, which may favor the passive targeting of these nanoparticles to the tumor tissue through the EPR effect [5,6]. Furthermore, nanoparticles smaller than 5 nm are rapidly removed from the circulation via renal clearance, while particles larger than 200 nm are more likely to be removed by the mononuclear phagocyte system [30].

The hydrophobic conjugate showed a high affinity for the lipid matrix of the NLC with an encapsulation rate near 100%. *In vitro* release studies revealed a slow DOX release from DOX-hyd-TS/NLC at pH 7.4, while fast release occurred at acidic conditions due to the pH-sensitive hydrazone bond. This indicates that the conjugate remains stable at physiological pH, while DOX can be rapidly released under low pH conditions of tumor cells, especially in the internal compartments of endosomes. Similar findings were reported by Xiong et al. for a hydrazone prodrug of DOX and TS encapsulated in TPGS micelles [15]. This

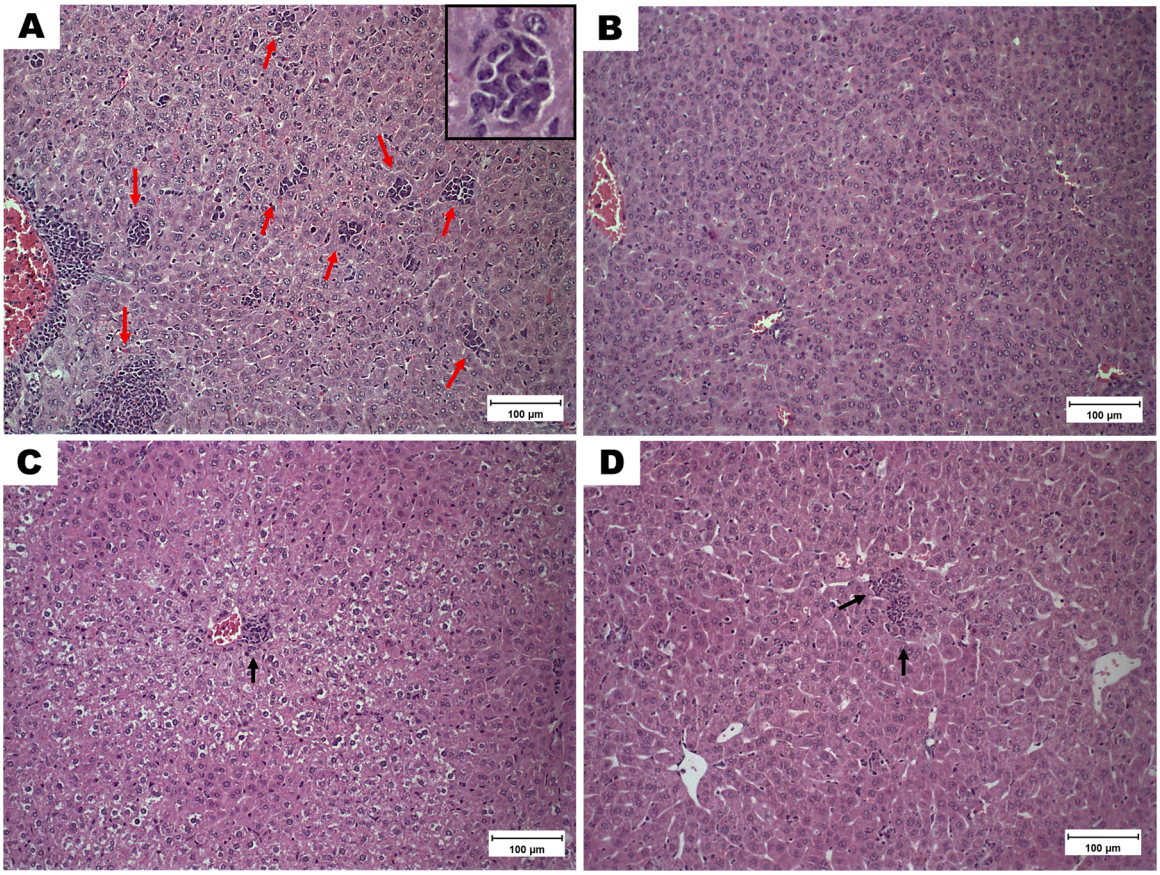

Fig. 8. Histological sections of the liver of 4T1 tumor-bearing BALB/c mice treated with blank-NLC (A), DOX solution (B), Lip-DOX (C), and DOX-hyd-TS/NLC (D). Hematoxylin-eosin staining. Original magnification x 20. Red arrows indicate metastasis (inset: metastatic focus – amplification 40 x), and black arrows represent inflammatory cells infiltration in the liver.

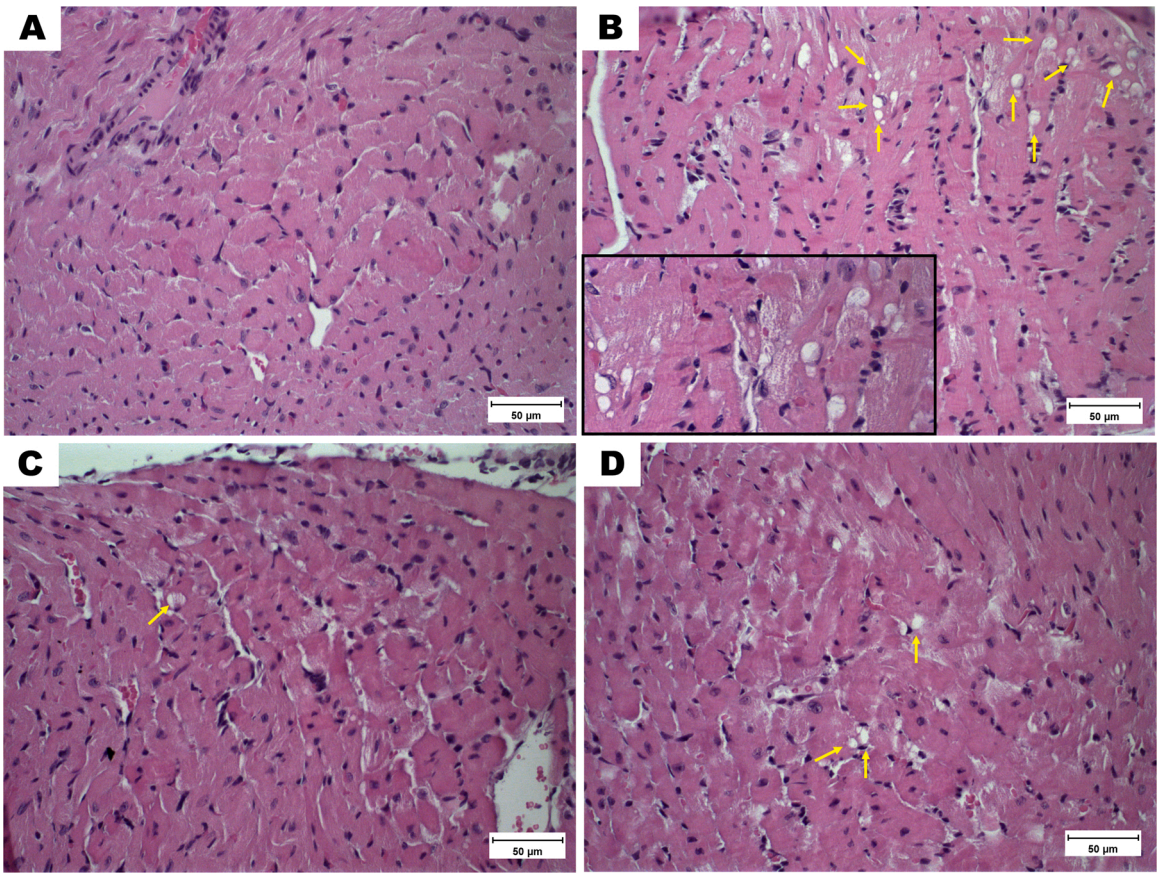

Fig. 9. Histological sections of the heart of 4T1 tumor-bearing BALB/c mice treated with blank-NLC (A), DOX solution (B), Lip-DOX (C), and DOX-hyd-TS/NLC (D). Hematoxylin-eosin staining. Original magnification x 40. Yellow arrows indicate vacuolization in the heart (inset: vacuoles – amplification 60 x).

selective release profile makes the use of hydrazone linkages one of the most attractive and well-studied approaches to the delivery of anticancer drugs, including paclitaxel, docetaxel, and DOX [17,43].

Pharmacokinetic studies performed in mice after a single intravenous injection revealed an improved behavior for DOX-hyd-TS/NLC, confirming that the chemical conjugation with TS increased DOX retention in the NLC. Previous studies have shown that the synthesis of DOX derivatives and encapsulation in lipid nanocarriers can prolong blood circulation, enhance tumor accumulation, and reduce off-target toxicity. Ni et al. produced an NLC formulation loading vincristine and a hydrolyzable prodrug of DOX and gemcitabine that showed better pharmacokinetics than DOX and greater antitumor efficacy in a lymph cancer mouse model [44]. Câmara et al. also described an acid-sensitive hydrophobic DOX prodrug encapsulated in a nanoemulsion system as an approach to improve pharmacokinetics and reduce systemic toxicity of DOX [45].

Besides the better pharmacokinetics, cardiotoxicity studies showed that DOX-hyd-TS/NLC avoided the acute effects evoked by DOX. Repeated treatment with free DOX, reaching a cumulative dose of 25 mg/kg, resulted in prolonged QT interval and impaired left ventricular systolic function, with reduced ejection fraction, fractional shortening, and cardiac output. Several studies have reported similar short-term changes in cardiac function and electrical integrity of the heart after administration of free DOX [46–48]. On the other hand, treatment with DOX-hyd-TS/NLC for approximately two weeks did not alter the ECG signal or echocardiographic parameters. The role of nanomedicine in reducing chemotherapy-induced cardiotoxicity is widely known [3,49]. Nanocarriers can modulate both pharmacokinetic and pharmacodynamic profiles of drugs, thereby decreasing their delivery and toxicity to non-target organs. Moreover, they accumulate to a lesser extent in the heart than free drugs since they cannot cross the tight junctions of myocardial vessels, which minimizes their cardiotoxic effects [3,50].

In vivo studies in 4T1 tumor-bearing mice showed that DOX-hyd-TS/NLC was more effective than free DOX in controlling tumor growth. Treatment with this formulation led to a tumor inhibition rate of 61%, against 44% for free DOX and 56% for Lip-DOX, a liposomal system similar to commercial Doxil®. Fernandes et al. reported similar findings for a DOX-loaded NLC system that also had superior antitumor efficacy than liposomes and the free drug in an animal model of breast cancer [51]. The excellent therapeutic performance of DOX-hyd-TS/NLC can be attributed to its improved pharmacokinetics and the pH-sensitive release of DOX, in addition to the adjuvant effects of DHA and TS. DHA induces cancer cell apoptosis, cell cycle arrest, and oxidative DNA damage through multiple mechanisms, including membrane incorporation, lipid peroxidation, and action on nuclear receptors [40,52]. TS also has anticancer properties due to the induction of apoptosis, inhibition of cell proliferation, and disruption of DNA synthesis [12,34]. Moreover, several in vitro and animal studies have shown that the combination of DHA or TS with DOX can enhance anticancer efficacy and reduce therapy-associated side effects [10–12,15].

Treatment with free DOX resulted in clinical signs of toxicity and a high mortality rate during the investigation of acute cardiotoxicity and antitumor efficacy. Hematologic, biochemical, and histopathologic analyses confirmed the damage caused by DOX to the bone marrow, liver, and heart. DOX is a myelosuppressive drug and can directly induce platelet cytotoxicity through ROS generation, reducing glutathione levels, and depleting thiol proteins [53]. The liver is a common site for DOX-induced cell death and tissue damage. The metabolism of high DOX concentrations results in the production of many ROS, which causes DNA damage, lipid peroxidation, and reduced levels of vitamin E [27,54]. In turn, cardiotoxicity is its most severe and debilitating toxic effect. Acute DOX cardiotoxicity is characterized by cardiomyocyte

degeneration, QT interval prolongation, and increased plasma cardiac markers, such as CK-MB, released in the early response to cardiac injury [46,47].

On the other hand, the administration of DOX-hyd-TS/NLC and Lip-DOX could prevent or reduce most of these toxic effects. In previous studies carried out by our group, both NLC and liposomes radiolabeled with technetium-99 m showed an altered biodistribution profile compared to DOX solution, with increased accumulation in the tumor site and reduced uptake by non-target organs, which justifies the lower toxicity of these systems concerning the free drug [20,46]. Interestingly, DOX-hyd-TS/NLC showed a better toxicity profile than the liposomal formulation, reflected in lower weight loss and unchanged liver enzymes at the end of treatment. These results reinforce an essential role for the combination of DHA and TS in reducing the toxic effects of DOX, in line with our previous report [9], and confirm that the co-encapsulation of these compounds in nanocarriers is an exciting approach for cancer therapy.

5. Conclusion

Hydrophobic DOX derivatives were synthesized in good yields by covalent conjugation to TS via an amide or hydrazone bond. *In vitro* cell analyses indicated that DOX-ami-TS had low cytotoxicity against 4T1 tumor cells, while DOX-hyd-TS effectively reduced cell viability. The hydrazone conjugate was successfully incorporated into a DHA-based NLC, which showed reduced particle size, homogeneous size distribution, and high encapsulation efficiency. *In vitro* release studies revealed a controlled DOX release from the NLC, with increased drug release in the acidic environment due to the pH-sensitive hydrazone linkage. DOX-hyd-TS/NLC showed better pharmacokinetics than free DOX and DOX-TS ion-pair/NLC after intravenous injection in mice. It was also able to avoid the short-term cardiotoxic effects evoked by repeated DOX administration. In the 4T1 tumor-bearing mice model, this formulation presented significant efficacy in inhibiting tumor growth, reducing mice mortality, and decreasing DOX-induced toxicity to the heart and liver. Therefore, DOX-hyd-TS/NLC can be considered a promising formulation for breast cancer treatment.

CRediT authorship contribution statement

Eduardo Burgarelli Lages: Responsible for the conception and design, Data acquisition, Analysis, Interpretation of all studies, Writing and revising the article. **Renata Salgado Fernandes:** Contribution to the data acquisition, analysis, Interpretation of in vitro cell studies. **Marina Mol Sena Andrade:** Contribution to the synthesis of conjugates, Data acquisition, Analysis, Interpretation of NMR characterization. **Nitchawat Paiyabhroma:** Contribution to the data acquisition, Analysis, Interpretation of cardiotoxicity study. **Renata Barbosa de Oliveira:** Contribution to the synthesis of conjugates, Data acquisition, Analysis, Interpretation of NMR characterization, Revising the article for intellectual content. **Christian Fernandes:** Contribution to the data acquisition, Analysis, Interpretation of pharmacokinetic studies, Revising the article for intellectual content. **Geovanni Dantas Cassali:** Contribution to the data acquisition, Analysis, Interpretation of histologic analyses. **Pierre Sicard:** Contribution to the data acquisition, Analysis, Interpretation of cardiotoxicity study, Revising the article for intellectual content. **Sylvain Richard:** Contribution to the data acquisition, Analysis, Interpretation of cardiotoxicity study, Revising the article for intellectual content. **André Luís Branco de Barros:** Responsible for the conception and design, Data analysis, Interpretation, Drafting and revising the article for intellectual content. **Lucas Antônio Miranda Ferreira:** Responsible for the conception and design, Data analysis, Interpretation, Drafting and revising the article for intellectual content.

Conflict of interest statement

The authors declare that they have no conflicts of interest.

Acknowledgments

This work was supported by Conselho Nacional de Desenvolvimento Científico e Tecnológico (CNPq, Brazil), Coordenação de Aperfeiçoamento de Pessoal de Nível Superior (CAPES, Brazil), and Fundação de Amparo à Pesquisa do Estado de Minas Gerais (FAPEMIG, Brazil). The authors would like to thank the Center of Microscopy (CM-UFMG, Brazil) and Imagerie du Petit Animal de Montpellier (IPAM) (LRQA Iso9001; France Life Imaging (grant ANR-11-INBS-0006); IBISA; Fondation Leducq (RETP), I-Site Muse) for providing equipment and technical support for the cryo-TEM and cardiotoxicity analyses, respectively. In addition, E.B. Lages is grateful to FAPEMIG and CAPES for providing the scholarships.

Author's contributions

Eduardo Burgarelli Lages, André Luís Branco de Barros, and Lucas Antônio Miranda Ferreira conceived and designed the project; **Eduardo Burgarelli Lages**, **Renata Salgado Fernandes**, **Marina Mol Sena Andrade**, and **Nitchawat Paiyabhroma** performed all experiments; **Renata Barbosa de Oliveira**, **Christian Fernandes**, **Geovanni Dantas Cassali**, **Pierre Sicard**, **Sylvain Richard**, **André Luís Branco de Barros**, and **Lucas Antônio Miranda Ferreira** supervised and provided expertise. All authors have read and approved the manuscript.

Appendix A. Supporting information

Supplementary data associated with this article can be found in the online version at doi:10.1016/j.biopha.2021.112373.

References

[1] L. Zhao, B. Zhang, Doxorubicin induces cardiotoxicity through upregulation of death receptors mediated apoptosis in cardiomyocytes, Sci. Rep. 7 (2017) 44735, https://doi.org/10.1038/srep44735.
[2] C. Carvalho, R. Santos, S. Cardoso, S. Correia, P. Oliveira, M. Santos, P. Moreira, Doxorubicin: the good, the bad and the ugly effect, Curr. Med. Chem. 16 (2009) 3267–3285, https://doi.org/10.2174/092986709788803312.
[3] M. Cagel, E. Grotz, E. Bernabeu, M.A. Moretton, D.A. Chiappetta, Doxorubicin: nanotechnological overviews from bench to bedside, Drug Discov. Today 22 (2017) 270–281, https://doi.org/10.1016/j.drudis.2016.11.005.
[4] A. Shafei, W. El-Bakly, A. Sobhy, O. Wagdy, A. Reda, O. Aboelenin, A. Marzouk, K. El Habak, R. Mostafa, M.A. Ali, M. Ellithy, A review on the efficacy and toxicity of different doxorubicin nanoparticles for targeted therapy in metastatic breast cancer, Biomed. Pharmacother. 95 (2017) 1209–1218, https://doi.org/10.1016/j.biopha.2017.09.059.
[5] D. Kalyane, N. Raval, R. Maheshwari, V. Tambe, K. Kalia, R.K. Tekade, Employment of enhanced permeability and retention effect (EPR): nanoparticle-based precision tools for targeting of therapeutic and diagnostic agent in cancer, Mater. Sci. Eng. C. 98 (2019) 1252–1276, https://doi.org/10.1016/j.msec.2019.01.066.
[6] J. Fang, H. Nakamura, H. Maeda, The EPR effect: unique features of tumor blood vessels for drug delivery, factors involved, and limitations and augmentation of the effect, Adv. Drug Deliv. Rev. 63 (2011) 136–151, https://doi.org/10.1016/j.addr.2010.04.009.
[7] A. Khosa, S. Reddi, R.N. Saha, Nanostructured lipid carriers for site-specific drug delivery, Biomed. Pharmacother. 103 (2018) 598–613, https://doi.org/10.1016/j.biopha.2018.04.055.
[8] M. Haider, S.M. Abdin, L. Kamal, G. Orive, Nanostructured lipid carriers for delivery of chemotherapeutics: a review, Pharmaceutics 12 (2020) 288, https://doi.org/10.3390/pharmaceutics12030288.
[9] E.B. Lages, R.S. Fernandes, J. de, O. Silva, Â.M. de Souza, G.D. Cassali, A.L.B. de Barros, L.A. Miranda Ferreira, Co-delivery of doxorubicin, docosahexaenoic acid, and α-tocopherol succinate by nanostructured lipid carriers has a synergistic effect to enhance antitumor activity and reduce toxicity, Biomed. Pharmacother. 132 (2020), 110876, https://doi.org/10.1016/j.biopha.2020.110876.
[10] R.A. Siddiqui, K.A. Harvey, Z. Xu, E.M. Bammerlin, C. Walker, J.D. Altenburg, Docosahexaenoic acid: a natural powerful adjuvant that improves efficacy for anticancer treatment with no adverse effects, BioFactors 37 (2011) 399–412, https://doi.org/10.1002/biof.181.

[11] S. Serini, R.O. Vasconcelos, R.N. Gomes, G. Calviello, Protective effects of ω-3 PUFA in anthracycline-induced cardiotoxicity: a critical review, Int. J. Mol. Sci. 18 (2017) 2689, https://doi.org/10.3390/ijms18122689.

[12] K.N. Prasad, B. Kumar, X.D. Yan, A.J. Hanson, W.C. Cole, α-tocopheryl succinate, the most effective form of vitamin e for adjuvant cancer treatment: a review, J. Am. Coll. Nutr. 22 (2003) 108–117, https://doi.org/10.1080/07315724.2003.10719283.

[13] M.S. Oliveira, S.V. Mussi, D.A. Gomes, M.I. Yoshida, F. Frezard, V.M. Carregal, L.A. M. Ferreira, α-Tocopherol succinate improves encapsulation and anticancer activity of doxorubicin loaded in solid lipid nanoparticles, Colloids Surf. B Biointerfaces 140 (2016) 246–253, https://doi.org/10.1016/j.colsurfb.2015.12.019.

[14] N. Duhem, F. Danhier, V. Pourcelle, J.M. Schumers, O. Bertrand, C.S. Leduff, S. Hoeppener, U.S. Schubert, J.F. Gohy, J. Marchand-Brynaert, V. Préat, Self-assembling doxorubicin-tocopherol succinate prodrug as a new drug delivery system: synthesis, characterization, and in vitro and in vivo anticancer activity, Bioconjug. Chem. 25 (2014) 72–81, https://doi.org/10.1021/bc400326y.

[15] S. Xiong, Z. Wang, J. Liu, X. Deng, R. Xiong, X. Cao, Z. Xie, X. Lei, Y. Chen, G. Tang, A pH-sensitive prodrug strategy to co-deliver DOX and TOS in TPGS nanomicelles for tumor therapy, Colloids Surf. B Biointerfaces 173 (2019) 346–355, https://doi.org/10.1016/j.colsurfb.2018.10.012.

[16] X. Zeng, G. Liu, W. Tao, Y. Ma, X. Zhang, F. He, J. Pan, L. Mei, G. Pan, A drug-self-gated mesoporous antitumor nanoplatform based on pH-sensitive dynamic covalent bond, Adv. Funct. Mater. 27 (2017), 1605985, https://doi.org/10.1002/adfm.201605985.

[17] S.J. Sonawane, R.S. Kalhapure, T. Govender, Hydrazone linkages in pH responsive drug delivery systems, Eur. J. Pharm. Sci. 99 (2017) 45–65, https://doi.org/10.1016/j.ejps.2016.12.011.

[18] Z. Li, X. Shan, Z. Chen, N. Gao, W. Zeng, X. Zeng, L. Mei, Applications of surface modification technologies in nanomedicine for deep tumor penetration, Adv. Sci. 8 (2021), 2002589, https://doi.org/10.1002/advs.202002589.

[19] W. Cheng, X. Zeng, H. Chen, Z. Li, W. Zeng, L. Mei, Y. Zhao, Versatile polydopamine platforms: synthesis and promising applications for surface modification and advanced nanomedicine, ACS Nano 13 (2019) 8537–8565, https://doi.org/10.1021/acsnano.9b04436.

[20] R.S. Fernandes, J.O. Silva, H.A. Seabra, M.S. Oliveira, V.M. Carregal, J.M.C. Vilela, M.S. Andrade, D.M. Townsend, P.M. Colletti, E.A. Leite, V.N. Cardoso, L.A. M. Ferreira, D. Rubello, A.L.B. Barros, α- Tocopherol succinate loaded nano-structured lipid carriers improves antitumor activity of doxorubicin in breast cancer models in vivo, Biomed. Pharmacother. 103 (2018) 1348–1354, https://doi.org/10.1016/j.biopha.2018.04.139.

[21] G.A. Castro, A.L.L.R. Coelho, C.A. Oliveira, G.A.B. Mahecha, R.L. Oréfice, L.A. M. Ferreira, Formation of ion pairing as an alternative to improve encapsulation and stability and to reduce skin irritation of retinoic acid loaded in solid lipid nanoparticles, Int. J. Pharm. 381 (2009) 77–83, https://doi.org/10.1016/j.ijpharm.2009.07.025.

[22] S.V. Mussi, R.C. Silva, M.C. De Oliveira, C.M. Lucci, R.B. De Azevedo, L.A. M. Ferreira, New approach to improve encapsulation and antitumor activity of doxorubicin loaded in solid lipid nanoparticles, Eur. J. Pharm. Sci. 48 (2013) 282–290, https://doi.org/10.1016/j.ejps.2012.10.025.

[23] R.G. Strickley, Solubilizing excipients in oral and injectable formulations, Pharm. Res. 21 (2004) 201–230, https://doi.org/10.1023/B:PHAM.0000016235.32639.23.

[24] Y. Zhang, M. Huo, J. Zhou, S. Xie, PKSolver: An add-in program for pharmacokinetic and pharmacodynamic data analysis in Microsoft Excel, Comput. Methods Prog. Biomed. 99 (2010) 306–314, https://doi.org/10.1016/j.cmpb.2010.01.007.

[25] P. Sicard, T. Jouitteau, T. Andrade-Martins, A. Massad, G.R. de Araujo, H. David, L. Miquerol, P. Colson, S. Richard, Right coronary artery ligation in mice: a novel method to investigate right ventricular dysfunction and biventricular interaction, Am. J. Physiol. - Hear. Circ. Physiol. 316 (2019) 684–692, https://doi.org/10.1152/ajpheart.00573.2018.

[26] R.T. Branquinho, J. Roy, C. Farah, G.M. Garcia, F. Aimond, J.Y. Le Guennec, D. A. Saude-Guimarães, A. Grabe-Guimaraes, V.C.F. Mosqueira, M. De Lana, S. Richard, Biodegradable polymeric nanocapsules prevent cardiotoxicity of anti-trypanosomal lychnopholide, Sci. Rep. 7 (2017) 44998, https://doi.org/10.1038/srep44998.

[27] F.A. Boratto, M.S. Franco, A.L.B. Barros, G.D. Cassali, A. Malachias, L.A. M. Ferreira, E.A. Leite, Alpha-tocopheryl succinate improves encapsulation, pH-sensitivity, antitumor activity and reduces toxicity of doxorubicin-loaded liposomes, Eur. J. Pharm. Sci. 144 (2020), 105205, https://doi.org/10.1016/j.ejps.2019.105205.

[28] N.E. Everds, Hematology of the Laboratory Mouse, in: Mouse Biomed. Res., Elsevier Inc, 2007, pp. 133–170, https://doi.org/10.1016/B978-012369454-6/50059-5.

[29] S.A. duPre', K.W. Hunter, Murine mammary carcinoma 4T1 induces a leukemoid reaction with splenomegaly: association with tumor-derived growth factors, Exp. Mol. Pathol. 82 (2007) 12–24, https://doi.org/10.1016/j.yexmp.2006.06.007.

[30] E. Blanco, H. Shen, M. Ferrari, Principles of nanoparticle design for overcoming biological barriers to drug delivery, Nat. Biotechnol. 33 (2015) 941–951, https://doi.org/10.1038/nbt.3330.

[31] K.D. Ristroph, R.K. Prud'homme, Hydrophobic ion pairing: encapsulating small molecules, peptides, and proteins into nanocarriers, Nanoscale Adv. 1 (2019) 4207–4237, https://doi.org/10.1039/c9na00308h.

[32] A. Gamboa, N. Schüßler, E. Soto-Bustamante, P. Romero-Hasler, L. Meinel, J. O. Morales, Delivery of ionizable hydrophilic drugs based on pharmaceutical formulation of ion pairs and ionic liquids, Eur. J. Pharm. Biopharm. 156 (2020) 203–218, https://doi.org/10.1016/j.ejpb.2020.09.007.

[33] W. Li, X. Yi, X. Liu, Z. Zhang, Y. Fu, T. Gong, Hyaluronic acid ion-pairing nanoparticles for targeted tumor therapy, J. Control. Release 225 (2016) 170–182, https://doi.org/10.1016/j.jconrel.2016.01.049.

[34] J. Neuzil, Vitamin E succinate and cancer treatment: a vitamin E prototype for selective antitumour activity, Br. J. Cancer 89 (2003) 1822–1826, https://doi.org/10.1038/sj.bjc.6601360.

[35] L. Liang, L. Qiu, Vitamin E succinate with multiple functions: a versatile agent in nanomedicine-based cancer therapy and its delivery strategies, Int. J. Pharm. 600 (2021), 120457, https://doi.org/10.1016/j.ijpharm.2021.120457.

[36] X. Zhang, F. He, K. Xiang, J. Zhang, M. Xu, P. Long, H. Su, Z. Gan, Q. Yu, CD44-targeted facile enzymatic activatable chitosan nanoparticles for efficient antitumor therapy and reversal of multidrug resistance, Biomacromolecules 19 (2018) 883–895, https://doi.org/10.1021/acs.biomac.7b01676.

[37] J. Lu, C. Liu, P. Wang, M. Ghazwani, J. Xu, Y. Huang, X. Ma, P. Zhang, S. Li, The self-assembling camptothecin-tocopherol prodrug: an effective approach for formulating camptothecin, Biomaterials 62 (2015) 176–187, https://doi.org/10.1016/j.biomaterials.2015.05.046.

[38] B.S. Chhikara, N. Jean St., D. Mandal, A. Kumar, K. Parang, Fatty acyl amide derivatives of doxorubicin: synthesis and in vitro anticancer activities, Eur. J. Med. Chem. 46 (2011) 2037–2042, https://doi.org/10.1016/j.ejmech.2011.02.056.

[39] B.S. Chhikara, D. Mandal, K. Parang, Synthesis, anticancer activities, and cellular uptake studies of lipophilic derivatives of doxorubicin succinate, J. Med. Chem. 55 (2012) 1500–1510, https://doi.org/10.1021/jm201653u.

[40] E.A. Song, H. Kim, Docosahexaenoic acid induces oxidative DNA damage and apoptosis, and enhances the chemosensitivity of cancer cells, Int. J. Mol. Sci. 17 (2016) 1257, https://doi.org/10.3390/ijms17081257.

[41] Y. Adkins, D.S. Kelley, Mechanisms underlying the cardioprotective effects of omega-3 polyunsaturated fatty acids, J. Nutr. Biochem 21 (2010) 781–792, https://doi.org/10.1016/j.jnutbio.2009.12.004.

[42] E.B. Lages, G.S.M. Borges, G.A.C. Goulart, L.A.M. Ferreira, Nanomedicine to deliver docosahexaenoic acid: potential applications to improve health, Nanomedicine 16 (2021) 1549–1552, https://doi.org/10.2217/nnm-2021-0128.

[43] S. Manchun, C.R. Dass, P. Sriamornsak, Targeted therapy for cancer using pH-responsive nanocarrier systems, Life Sci. 90 (2012) 381–387, https://doi.org/10.1016/j.lfs.2012.01.008.

[44] S. Ni, L. Qiu, G. Zhang, H. Zhou, Y. Han, Lymph cancer chemotherapy: delivery of doxorubicin-gemcitabine prodrug and vincristine by nanostructured lipid carriers, Int. J. Nanomed. 12 (2017) 1565–1576, https://doi.org/10.2147/IJN.S120685.

[45] A.L. Dos Santos Câmara, G. Nagel, H.R. Tschiche, C.M. Cardador, L.A. Muehlmann, D.M. De Oliveira, P.Q. Alvim, R.B. Azevedo, M. Calderón, J.P.F. Longo, Acid-sensitive lipidated doxorubicin prodrug entrapped in nanoemulsion impairs lung tumor metastasis in a breast cancer model, Nanomedicine 12 (2017) 1751–1765, https://doi.org/10.2217/nnm-2017-0091.

[46] J. de Oliveira Silva, R.S. Fernandes, C.M. Ramos Oda, T.H. Ferreira, A.F. Machado Botelho, M. Martins Melo, M.C. de Miranda, D. Assis Gomes, G. Dantas Cassali, D. M. Townsend, D. Rubello, M.C. Oliveira, A.L.B. de Barros, Folate-coated, long-circulating and pH-sensitive liposomes enhance doxorubicin antitumor effect in a breast cancer animal model, Biomed. Pharmacother. 118 (2019), 109323, https://doi.org/10.1016/j.biopha.2019.109323.

[47] M. Pecoraro, A. Rodríguez-Sinovas, S. Marzocco, M. Ciccarelli, G. Iaccarino, A. Pinto, A. Popolo, Cardiotoxic effects of short-term doxorubicin administration: Involvement of connexin 43 in calcium impairment, Int. J. Mol. Sci. 18 (2017) 2121, https://doi.org/10.3390/ijms18102121.

[48] L. Zhang, K. Zhu, H. Zeng, J. Zhang, Y. Pu, Z. Wang, T. Zhang, B. Wang, Resveratrol solid lipid nanoparticles to trigger credible inhibition of doxorubicin cardiotoxicity, Int. J. Nanomed. 14 (2019) 6061–6071, https://doi.org/10.2147/IJN.S211130.

[49] G.S.M. Borges, E.B. Lages, P. Sicard, L.A.M. Ferreira, S. Richard, Nanomedicine in oncocardiology: contribution and perspectives of preclinical studies, Front. Cardiovasc. Med. 8 (2021), 690533, https://doi.org/10.3389/fcvm.2021.690533.

[50] M. Fojtu, J. Gumulec, T. Stracina, M. Raudenska, A. Skotakova, M. Vaculovicova, V. Adam, P. Babula, M. Novakova, M. Masarik, Reduction of doxorubicin-induced cardiotoxicity using nanocarriers: a review, Curr. Drug Metab. 18 (2017) 237–263, https://doi.org/10.2174/1389200218666170105165444.

[51] R.S. Fernandes, J.O. Silva, L.O.F. Monteiro, E.A. Leite, G.D. Cassali, D. Rubello, V. N. Cardoso, L.A.M. Ferreira, M.C. Oliveira, A.L.B. de Barros, Doxorubicin-loaded nanocarriers: A comparative study of liposome and nanostructured lipid carrier as alternatives for cancer therapy, Biomed. Pharmacother. 84 (2016) 252–257, https://doi.org/10.1016/j.biopha.2016.09.032.

[52] M. Newell, K. Baker, L.M. Postovit, C.J. Field, A critical review on the effect of docosahexaenoic acid (Dha) on cancer cell cycle progression, Int. J. Mol. Sci. 18 (2017) 1784, https://doi.org/10.3390/ijms18081784.

[53] E.J. Kim, K.M. Lim, K.Y. Kim, O.N. Bae, J.Y. Noh, S.M. Chung, S. Shin, Y.P. Yun, J. H. Chung, Doxorubicin-induced platelet cytotoxicity: a new contributory factor for doxorubicin-mediated thrombocytopenia, J. Thromb. Haemost. 7 (2009) 1172–1183, https://doi.org/10.1111/j.1538-7836.2009.03477.x.

[54] P.L. Prasanna, K. Renu, A. Valsala Gopalakrishnan, New molecular and biochemical insights of doxorubicin-induced hepatotoxicity, Life Sci. 250 (2020), 117599, https://doi.org/10.1016/j.lfs.2020.117599.